Characterization of Layered Silicate Dispersion in Polymer Nanocomposites Using Fourier Transform Infrared Spectroscopy

Xingui Zhang, Sowrirajalu Bhuvana, Leslie S. Loo

School of Chemical and Biomedical Engineering, Nanyang Technological University, Singapore 637459, Singapore

Received 11 February 2011; accepted 23 September 2011
DOI 10.1002/app.36266
Published online 28 December 2011 in Wiley Online Library (wileyonlinelibrary.com).

ABSTRACT: Fourier transform infrared (FTIR) spectroscopy was used to characterize the state of dispersion of layered silicate in polymer nanocomposites. The nanocomposite samples were based on poly(hexamethylene isophthalamide) and montmorillonite nanoclay prepared by melt intercalation. The infrared spectra of Si—O stretching bands between 1150 and 960 cm^{-1} are found to be very sensitive to the extent of nanoclay dispersion at the molecular level. Increased level of nanoclay delamination resulted in significant changes to the out-of-plane a_1^1 mode at 1082 cm^{-1} and the two in-plane modes b_1^1 and b_2^2 at 1050 and 1030 cm^{-1}, respectively. The a_1^1 mode shows a substantial increase in intensity and shifts toward lower wave numbers. The bandwidths of the b_1^1 and b_2^2 modes are reduced significantly. The b_2^2 mode also shifts toward higher wave numbers in exfoliated nanoclay. Hence, FTIR can complement other methods to characterize the morphology of polymer nanocomposites. © 2011 Wiley Periodicals, Inc. J Appl Polym Sci 125: E175–E180, 2012

Key words: layered silicate; dispersion; infrared spectroscopy; nanocomposites; amorphous polyamide

INTRODUCTION

Recent interest in polymer/layered silicate nanocomposites is motivated by the possibility of achieving enhanced properties at lower nanofiller loading.[1,2] For instance, the addition of only 5 wt % montmorillonite (MMT) to polyamide has resulted in an enhancement of its mechanical properties,[3,4] increased its heat distortion temperature,[5] and improved its barrier properties.[6] The degree of nanoclay dispersion has been found to be critical in determining the final properties of polymer nanocomposites.[2,7] To improve nanoclay dispersion in polymer matrix, organic modification of the clay surface via cation exchange has been used to expand the clay interlayer spacing and increase compatibility with polymer matrix.[8]

Most of the nanoclay used in polymer nanocomposites is MMT. MMT forms small crystallites of a lamellar structure comprising of repeated sheets of one central alumina octahedral sheet sandwiched between two parallel silica tetrahedral sheets, condensed into one unit layer designated as "tetrahedral-octahedral-tetrahedral."[9] Generally, the dispersion state of MMT in polymer nanocomposites is characterized by wide-angle X-ray diffraction (WAXD) and transmission electron microscopy (TEM).[10,11] However, these techniques have some shortcomings.[12,13] One limitation of WAXD is that it can only determine the nanoclay interlayer spacing within 1−4 nm in polymer nanocomposites. Hence, the absence of clay diffraction peak is not necessarily conclusive evidence for an exfoliated structure.[9] On the other hand, TEM gives a more direct visual indication of the dispersion state of the clay but it only reveals the morphology in a very small region.[14]

Spectroscopic tools such as Fourier transform infrared (FTIR) can be alternative techniques to characterize nanoclay dispersion because of their nondestructive nature and sample preparation is minimal.[13,15] The Si—O stretching modes of MMT in FTIR spectra are very sensitive to the distortion of the tetrahedral structure.[16] To the authors' knowledge, very little research has been devoted to investigating nanoclay MMT dispersion using infrared spectroscopy. Cole has studied MMT dispersion in high-density polyethylene and polypropylene.[13] In his study, however, a compatibilizer has been used in the synthesis of the polymer nanocomposites. Hence, it was not clear if the observed changes in the Si—O vibrational bands were due to the increase in interlayer distance or the interactions between nanoclay and compatibilizing agent.[13] Loo and

Correspondence to: L. S. Loo (ssloo@ntu.edu.sg).
Contract grant sponsor: Nanyang Technological University.

TABLE I
Material Properties of the Nanoclay and Surfactants Used in This Study

Nanoclay	Supplier designation	Specifications
NaMMT	*Cloisite Na*$^+$	92.6 CEC[a], d_{001} spacing = 1.05 nm
30BMMT	*Cloisite 30B*: Methyl, tallow, bis-2-hydroxyethyl quaternary ammonium chloride organoclay	90 CEC, organic content = 28.4 wt %, d_{001} spacing = 1.84 nm
10AMMT	*Cloisite 10A*:Dimethyl, benzyl, hydrogenated tallow quaternary ammonium chloride organoclay	125 CEC, organic content = 36.9 wt %, d_{001} spacing = 1.95 nm

[a] CEC indiactes cation exchange capacity in mequiv/100g.

Gleason[17] have also used FTIR to determine MMT orientation distribution in polymer nanocomposites, but they did not study the degree of dispersion. Our study will focus on the feasibility of determining nanoclay dispersion using FTIR analysis.

MATERIALS AND METHODS

Poly(hexamethylene isophthalamide) pellets were obtained from Lanxess (Singapore) under the product trade name Durethan T40. The polymer will be abbreviated as aPA in subsequent discussions. This is a completely amorphous polyamide.

Pristine sodium MMT nanoclay and two types of MMT-based organoclay were supplied by Southern Clay Products (Gonzales, TX). They are abbreviated as NaMMT, 30BMMT, and 10AMMT, respectively. The chemical names of the surfactants are given in Table I. Prior to blending the polymer and nanoclay, they were first dried in a vacuum oven at 80°C for at least 12 h. The solvent 1,1,1,3,3,3-hexafluoro-2-propanol (HFIP, 99.8% purity) was purchased from Sigma-Aldrich Pte Ltd (Singapore) and used as received.

The polymer/clay nanocomposites were prepared via a two-step melt blending process using a Haake Polydrive mixer in a nitrogen atmosphere according to the method described in a previous article.[18] For aPA containing nanoclay, polymer nanocomposites with nominal content of 5 and 10 wt % MMT (wt % excludes surfactants) were prepared. The pure aPA and the polymer nanocomposites were then compressed into films (approximately 150 ± 5 μm thickness) at 220°C using a Carver Press (Model 4128).

WAXD measurements were performed at room temperature on a Siemens D5005 X-ray diffractometer using Cu Kα radiation (λ = 0.1542 nm). The scanning rate was 1° per min for values of 2θ between 1° and 10°.

TEM was used to observe the dispersion of clay layers in the polymer matrix. Thin sections of 50 nm in thickness were cut from the nanocomposites at room temperature using a Leica ultramicrotome with a diamond knife. The sections were then examined using a JEOL 3010 TEM instrument at an acceleration voltage of 200 kV.

Sample preparation for FTIR analysis

For infrared analysis, the polymer/nanoclay nanocomposites were first dissolved in HFIP to form a 2 wt % solution. A film was then prepared by solvent casting onto a potassium bromide (KBr) window. After evaporation of the majority of the solvent at room temperature, the KBr window with the film was placed in a vacuum oven at 80°C for at least 24 h to remove residual solvent. The KBr window was then immediately transferred to the infrared spectrometer for analysis. Dried nanoclay powder mixed with KBr powder and then compressed into pellet form was also used as control for infrared analysis.

FTIR characterization

FTIR spectra were recorded at room temperature using a deuterated triglycine sulfate detector on a Nicolet Model 5700 spectrometer. The resolution was 2 cm^{-1}. A dry nitrogen purge was used to minimize absorption due to water.[19] All the samples were sufficiently thin to be within the absorbance range where the Beer–Lambert law was obeyed.[20] Curve fitting of the spectra was carried out with Originlab 7.5 software to determine the position, height, and area of each peak.

RESULTS AND DISCUSSION

The infrared spectra of nanoclay powders

Figure 1 shows the spectra of dried NaMMT, and organoclay 30BMMT and 10AMMT powders in the Si—O stretching region from 1150 to 960 cm^{-1}. All the spectra have been normalized to the peak height of the 10AMMT clay so as to allow for comparison of the band shapes. The weak Si—O stretching peak at 1100 cm^{-1} represents the in-plane (parallel) vibrations b_1^2 and b_1^3 (a linear combination of these) while the one at 1082 cm^{-1} represents the out-of-plane (perpendicular) vibration mode a_1^1.[12,21] The two strong peaks at 1050 and 1030 cm^{-1} also represent in-plane vibration modes b_1^1 and b_2^2, respectively.[12,21] Following the convention of Yan et al.,[22] the four bands are labeled I, II, III, and IV, respectively.

WAXD results for NaMMT, 30BMMT, and 10AMMT gave peaks at 2θ = 8.45° (d_{001} = 1.05 nm),

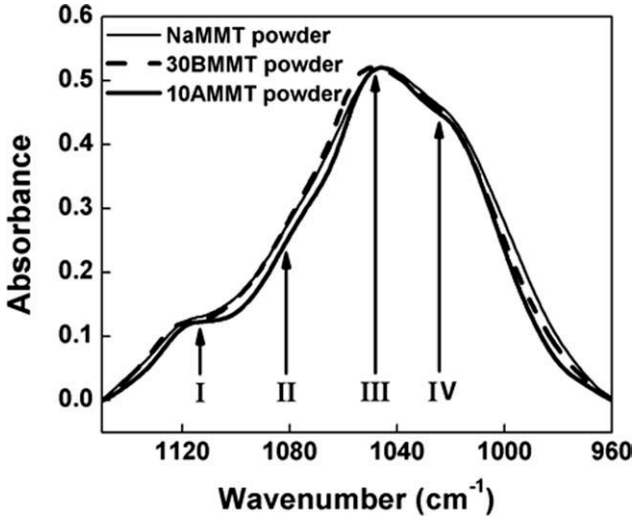

Figure 1 FTIR spectra of NaMMT, 30BMMT, and 10AMMT powder (normalized by height). Peaks I, II, III, and IV are located at 1100, 1082, 1050, and 1030 cm^{-1}, respectively.

4.81° (d_{001} = 1.84 nm), and 4.53° (d_{001} = 1.95 nm), respectively, corresponding to the d_{001} spacing given Table I. The expansion of the nanoclay galleries observed for 30BMMT and 10AMMT is due to the intercalation of the surfactants. However, from Figure 1, it is observed that the infrared spectra of both organoclays are similar to that of pristine clay. This shows that the intercalated organic surfactants do not affect appreciably the absorption bands of the agglomerated nanoclay powders.

The infrared spectra of nanoclay in aPA matrix

The morphology of aPA/NaMMT, aPA/30BMMT, and aPA/10AMMT polymer nanocomposites prepared by melt intercalation has been reported in a previous publication.[18] Figure 2(a) shows the WAXD patterns of aPA and its nanocomposites. For all the aPA/NaMMT hybrids, WAXD and TEM results indicated that the clay particles agglomerated together. Figure 2(b) shows a TEM image for aPA/NaMMT hybrid containing 5.03 wt % MMT. WAXD analysis and TEM images showed that the nanoclay in aPA/30BMMT nanocomposites containing 4.96 and 10.54 wt % MMT was fully delaminated and uniformly dispersed in the polymer matrix.[18] Figure 2(c) shows the TEM image of well-dispersed nanoclay in

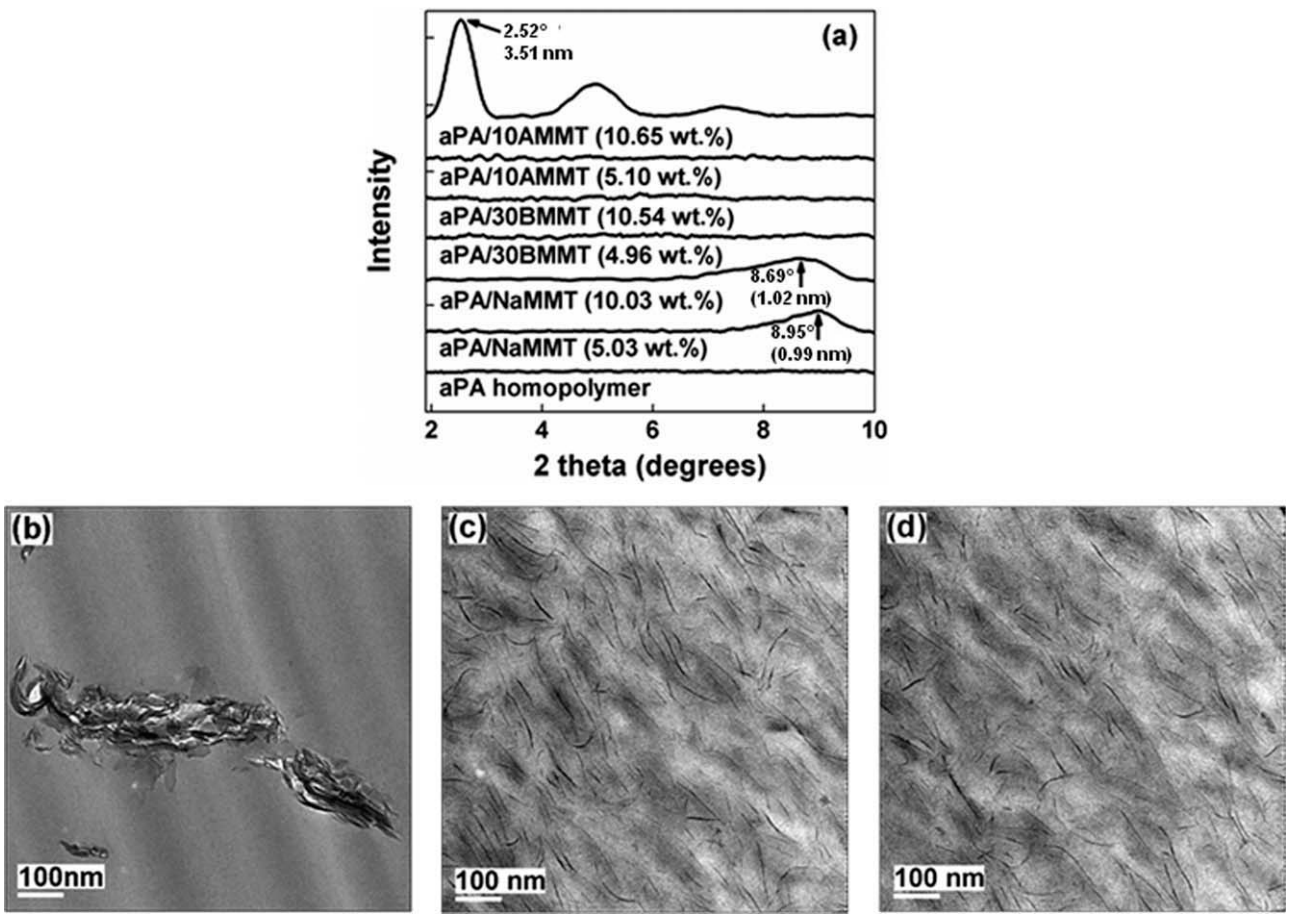

Figure 2 (a) WAXD patterns for aPA and its nanocomposites. TEM images of (b) aPA/NaMMT containing 5.03 wt % MMT, (c) aPA/30BMMT containing 4.96 wt % MMT, and (d) aPA/10AMMT containing 5.10 wt % MMT.

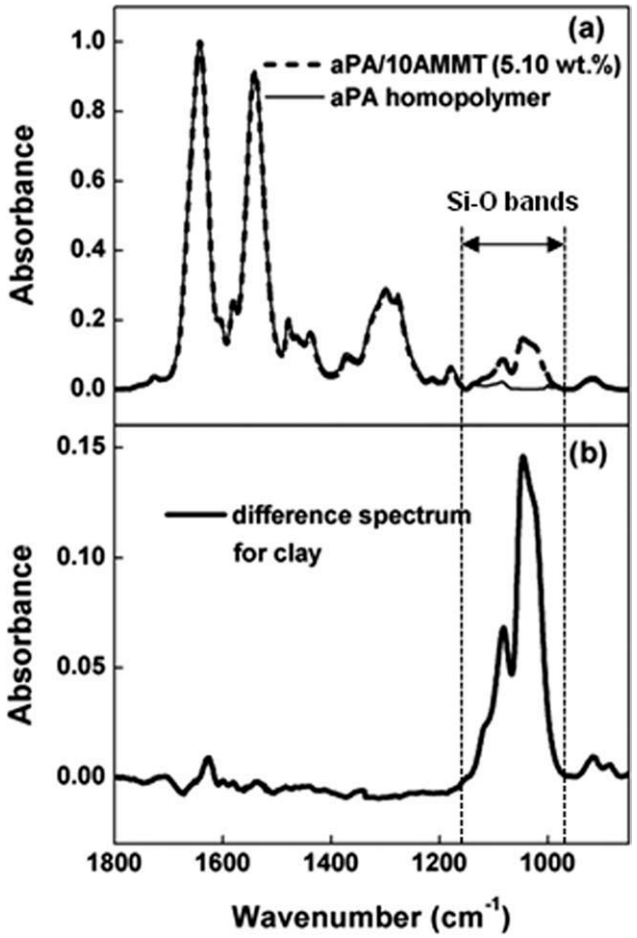

Figure 3 (a) FTIR spectra of aPA (thin continuous line) and aPA/10AMMT nanocomposite with 5.10 wt % MMT (thick dashed line) in the range 1800–850 cm^{-1}. (b) Difference spectrum obtained by subtraction, showing the clay absorption peaks.

aPA/30BMMT with 4.96 wt % MMT. In the aPA/10MMT system, WAXD and TEM data showed that at 5.10 wt % MMT content, an exfoliated morphology was also obtained as shown in Figure 2(d). However, for aPA/10AMMT containing 10.65 wt % MMT, the higher concentration of nanoclay resulted in a mixed exfoliated/intercalated morphology.[18]

To perform FTIR analysis, the melt-blended polymer nanocomposites were first dissolved in organic solvent HFIP and then cast on KBr windows. Hence, it is important to ensure that the solvent-casting process did not influence the clay dispersion. X-ray diffraction measurements of the solvent-cast films exhibited similar WAXD patterns as the melt-blended hybrids, indicating that the solvent-casting process did not affect the nanocomposite morphology.

Figure 3(a) shows the FTIR spectra of aPA polymer and aPA/10AMMT nanocomposite containing 5.10 wt % MMT. The Si—O stretching bands show up between 1150 and 960 cm^{-1}. Due to the completely amorphous nature of the polymer, the Si—O stretching peaks can be easily isolated by spectra subtraction of the aPA spectrum from the nanocomposite spectrum. To accomplish this, a flat baseline was first drawn from 1800 to 850 cm^{-1} for all the infrared spectra. The spectra were then normalized by height before spectra subtraction was performed.[13] Figure 3(b) shows the resulting difference spectrum of organoclay 10AMMT containing 5.10 wt % MMT.

The same procedure was repeated for all the other nanocomposites. Figure 4(a) compares the difference spectra of Si—O stretching vibrations for aPA nanocomposites containing NaMMT, 30BMMT, and 10AMMT at similar MMT loading (5 wt %). The agglomerated NaMMT nanoclay produced an absorption pattern, which is broader and has lower intensity compared with those from the delaminated organoclay 30BMMT and 10AMMT layers in aPA matrix.[15] The relative absorption intensities of peak II (1082 cm^{-1}) are also much higher for the well-dispersed nanoclay. These results are consistent with previous work with delaminated clay layers in water suspension, in which the Si—O absorption bands became narrow and increased in intensity,[16] while peak II became prominent.[22] Furthermore, Johnston and Premachandra[23] have observed a well-separated peak II for single MMT layers.

Figure 4(b–d) shows the respective nonlinear least-squares regression of the spectra in the Si—O stretching region for NaMMT, 30BMMT, and 10AMMT in aPA. All the spectra were baseline corrected and fitted with four symmetric Gaussian peaks allowing the peak positions, heights, and $W_{1/2}$ (full width at half height) to vary.[22] Table II lists the curve-fitting results for peaks II, III, and IV.

From Table II, the curve fitting results show that the frequency of peak II for NaMMT is approximately 1095 cm^{-1}, which is about 15 cm^{-1} higher than those for the exfoliated organoclay ($\sim$ 1080 cm^{-1}). The second-derivative curves of these Si—O stretching spectra also confirmed the location of peak II at 1095 cm^{-1} for NaMMT and 1080 cm^{-1} for organoclay, respectively. For peak II, the values of $W_{1/2}$ all fall within the range of 23.9–30.9 cm^{-1} in the three nanoclay systems, regardless of the dispersion morphology. Furthermore, it is observed that in the exfoliated systems, the intensity of peak II relative to the maximum peak height of Si—O stretch is much higher than for the agglomerated NaMMT system. This behavior can also be observed in Figure 4(b–d).[24] This indicates that the intensity of the out-of-plane Si—O band is particularly sensitive to the interlayer distance of nanoclay.[13]

Table II shows that peaks III and IV of the delaminated 30BMMT and 10AMMT layers, respectively, are significantly narrower than those of the NaMMT agglomerates. The difference is more prominent for peak III, whose $W_{1/2}$ has a value of 54.2 cm^{-1} in

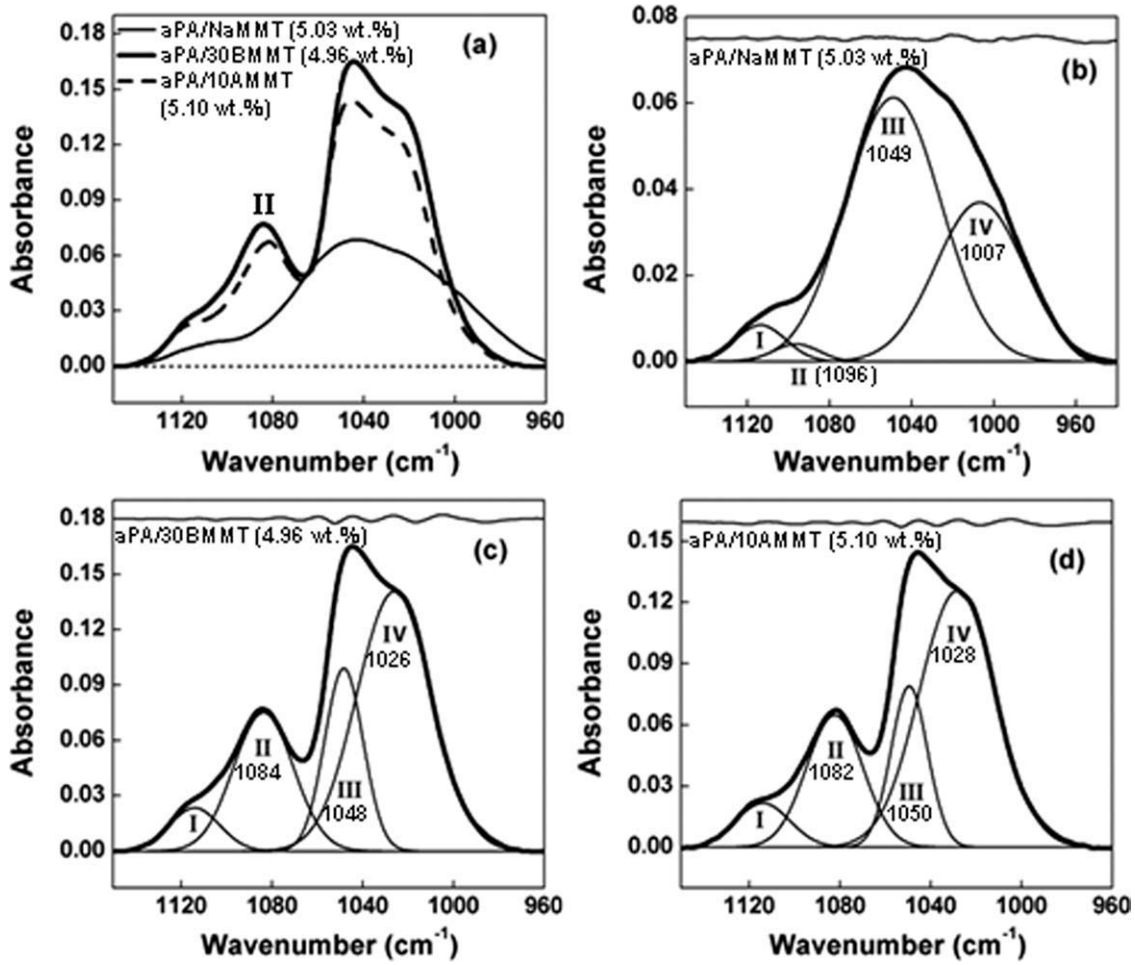

Figure 4 (a) FTIR difference spectra of the Si—O stretching region for aPA nanocomposites containing NaMMT, 30BMMT, and 10AMMT at 5 wt % clay loading. (b), (c), and (d). Nonlinear least-squares regression of the Si—O stretching region for aPA nanocomposites containing NaMMT, 30BMMT, and 10AMMT, respectively. Peaks II, III, and IV as well as their peak positions (to the nearest whole wave number) are indicated. The curve above each spectrum shows the difference between the best fit curve and actual data.

TABLE II
Curve-Fitting Results of the Si—O Stretching Region of Nanoclay in aPA

	NaMMT[a]		30BMMT[a]		10AMMT[a]	
Si—O stretching bands	5.03 wt %	10.03 wt %	4.96 wt %	10.54 wt %	5.10 wt %	10.65 wt %
Maximum height	0.068	0.134	0.165	0.331	0.145	0.308
Peak II						
Frequency (cm^{-1})	1096.4	1095.5	1083.7	1081.9	1082.3	1080.7
$W_{1/2}$ (cm^{-1})	25.7	23.9	30.9	29.6	28.8	27.1
Relative intensity[b]	0.06	0.06	0.46	0.34	0.45	0.34
Peak III						
Frequency (cm^{-1})	1049.0	1047.6	1048.3	1049.5	1049.5	1050.4
$W_{1/2}$ (cm^{-1})	54.2	54.5	19.6	18.1	18.5	17.0
Relative intensity[b]	0.90	0.88	0.62	0.53	0.56	0.45
Peak IV						
Frequency (cm^{-1})	1006.9	1004.3	1026.1	1028.5	1028.3	1030.6
$W_{1/2}$ (cm^{-1})	50.5	53.6	38.4	41.6	39.2	43.8
Relative intensity[b]	0.55	0.57	0.86	0.86	0.87	0.89

[a] The clay contents are based on MMT only.
[b] The relative intensity is the ratio of the height of the respective peak (II or III or IV) to the maximum peak height of the Si—O stretching absorption.

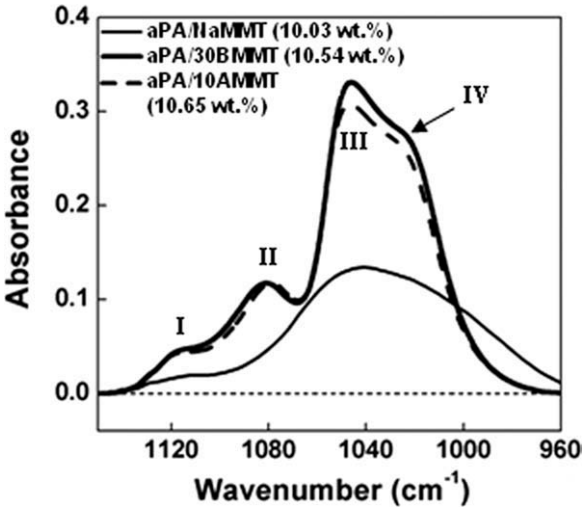

Figure 5 Comparison of FTIR spectra in the Si—O stretching region for NaMMT, 30BMMT, and 10AMMT in aPA matrix containing 10 wt % MMT.

NaMMT nanocomposite but drops to approximately 19 cm^{-1} in 30BMMT and 10AMMT (a 65% decrease). The width of peak IV shows a more modest decrease from approximately 50.5 to 39 cm^{-1}. For peak IV, there is also a significant peak shift toward higher wave numbers (from approximately 1006 to 1026 cm^{-1}) in the well-dispersed nanoclay. Furthermore, Table II shows that in the NaMMT system, peak III has a higher relative intensity than peak IV, but the situation is completely reversed in exfoliated 30BMMT and 10AMMT hybrids. This shows that the state of dispersion of the nanoclay affects the intensity of peaks III and IV relative to each other.

Figure 5 shows the spectra of Si—O stretching vibrations for the three nanoclay in aPA at 10 wt % MMT loading. Table II also lists the curve-fitting results of peaks II, III, and IV for the three aPA nanocomposites with 10 wt % MMT loading. In NaMMT system, the curve-fitting data do not differ by more than 3.1 cm^{-1} for both peak position and $W_{1/2}$ regardless of the filler content. However, with the addition of more organoclay, the relative intensity of peak II decreases in 10 wt % aPA/30BMMT and aPA/10AMMT compared with the 5 wt % MMT hybrids. Furthermore, for the aPA nanocomposites containing 30BMMT and 10AMMT, the widths of peak IV at 10 wt % MMT are higher than the respective values at 5 wt % MMT content. This is in contrast to the WAXD results in Figure 2(a), which did not show any difference for aPA/30BMMT containing 4.96 and 10.54 wt % MMT.[18] The broadened Si—O stretching absorption and the weakened peak II in the organoclay systems can be attributed to the decreased nanoclay interlayer distance due to the increased nanofiller density in the 10 wt % MMT hybrids. Hence, it is possible to relate FTIR spectra of Si—O stretching peaks to the extent of nanoclay delamination at the molecular level.[13] This shows that spectroscopic analysis can be more sensitive than X-ray diffraction for the characterization of exfoliated nanoclay morphology.[22]

SUMMARY

The infrared spectroscopic study of a novel amorphous polyamide/MMT nanocomposite shows that the FTIR spectra of Si—O stretching vibrations are sensitive to the extent of nanoclay dispersion at the molecular level. Increased level of nanoclay delamination resulted in significant changes to the out-of-plane a_1^1 mode (peak II) as well as the two in-plane modes b_1^1 and b_2^2 (peaks III and IV, respectively). Peak II shows a substantial increase in intensity and shifts toward lower wave numbers. The bandwidths of peaks III and IV are reduced significantly. Peak IV also shifts toward higher wave numbers in exfoliated nanoclay. Hence, the FTIR method can complement the existing techniques such as TEM and WAXD for characterization of polymer nanocomposite morphology.

The authors thank Prof. Mary Chan and Ms Tan Ruoshan for the use of their materials and equipment.

References

1. Fornes, T. D.; Hunter, D. L.; Paul, D. R. Macromolecules 2004, 37, 1793.
2. Rao, Y. Q.; Pochan, J. M. Macromolecules 2007, 40, 290.
3. Kim, E. S.; Shim, J. H.; Woo, J. Y.; Yoo, K. S.; Yoon, J. S. J Appl Polym Sci 2010, 117, 809.
4. Fornes, T. D.; Paul, D. R. Macromolecules 2004, 37, 7698.
5. Kojima, Y.; Usuki, A.; Kawasumi, M.; Okada, A.; Kurauchi, T.; Kamigaito, O. J Polym Sci Part A Polym Chem 1993, 31, 1755.
6. Beatrice, C. A. G.; Branciforti, M. C.; Alves, R. M. V.; Bretasi, R. E. S. J Appl Polym Sci 2010, 116, 3581.
7. Kotek, J.; Kelnar, I.; Baldrian, J.; Slouf, M. J Appl Polym Sci 2008, 110, 3752.
8. Southern Clay Products, datasheet. Available at: http://www.scprod.com/.
9. Paul, D. R.; Robeson, L. M. Polymer 2008, 49, 3187.
10. Morgan, A. B.; Gilman, J. W. J Appl Polym Sci 2003, 87, 1329.
11. Vermogen, A.; Masenelli-Varlot, K.; Seguela, R.; Duchet-Rumeau, J.; Boucard, S.; Prele, P. Macromolecules 2005, 38, 9661.
12. Loo, L. S.; Gleason, K. K. Macromolecules 2003, 36, 2587.
13. Cole, K. C. Macromolecules 2008, 41, 834.
14. Morgan, A. B., Gilman, J. W.; Jackson, C. L. Macromolecules 2001, 34, 2735.
15. Ijdo, W. L., Kemnetz, S.; Benderly, D. Polym Eng Sci 2006, 46, 1031.
16. Lerot, L.; Low, P. F. Clays Clay Miner 1976, 24, 191.
17. Loo, L. S.; Gleason, K. K. Polymer 2004, 45, 5933.
18. Zhang, X. G.; Loo, L. S. J Polym Sci Part B Polym Phys 2008, 46, 2605.
19. Schroeder, L. R.; Cooper, S. L. J Appl Phys 1976, 47, 4310.
20. Skrovanek, D. J., Howe, S. E.; Painter, P. C.; Coleman, M. M. Macromolecules 1985, 18, 1676.
21. Farmer, V. C.; Russell, J. D. Spectrochim Acta 1964, 20, 1149.
22. Yan, L. B.; Roth, C. B.; Low, P. F. Langmuir 1996, 12, 4421.
23. .Johnston, C. T.; Premachandra, G. S. Langmuir 2001, 17, 3712.
24. Shewring, N. I. E.; Jones, T. J. G.; Maitlang, G.; Yarwood, J. J Colloid Interface Sci 1995, 176, 308.